Towards implementation of FMCW LiDAR with quadrature modulator architectures in generic InP photonic integration technology

B.S. Vikram[1], A. Meighan[1] , K.A. Williams[1], and V. Dolores-Calzadilla[1,2]

[1] Technical University of Eindhoven, Dept. of Electrical Engineering ,De Groene Loper 19, 5612 AP Eindhoven, The Netherlands

[2] Photonic Integration Technology Center, De Groene Loper 19, 5612 AP Eindhoven, The Netherlands

Two architectures with quadrature modulation in a generic InP platform are proposed for realizing frequency-modulated continuous-wave (FMCW) LiDAR. Simulations are used to compare the architectures in terms of tolerance to optical imbalances, insertion loss, chip footprint, and ease of control. The parallel architecture is more resilient to imbalances (~0.82 dB power imbalance for 20 dB ER) than the cascaded architecture (~0.63 dB power imbalance for 20 dB ER).

Introduction

Light detection and ranging (LiDAR) finds applications in motion perception and surveying in various applications such as autonomous vehicles [1] , robotics, and surveying atmosphere. Frequency-modulated continuous wave (FMCW) LiDAR provides simultaneous information on position and velocity in a single acquisition [1]. Implementation of LiDAR systems in integrated photonics provides significant gains in size, weight, power, and cost. InP photonics [2] can include monolithically integrated lasers, high bandwidth electro-optic phase modulators, and optical amplifiers, which makes it a proper candidate for the implementation of FMCW LiDAR systems. These systems have been implemented through direct modulation of the laser [3]. However, this technique produces a nonlinear chirp and needs a control loop for monitoring the frequency and ensuring chirp linearity[3].External modulation of the laser with quadrature or IQ modulators can generate FMCW signals with linear chirp[4]. The quadrature modulator is driven with radiofrequency chirp signals to synthesize the FMCW signal [4], and the modulator operates in a carrier-suppressed single sideband (CS-SSB) mode of operation at each frequency of the RF chirp. Range resolution ($\frac{speed\ of\ light}{2(Sweep\ Bandwidth)}$) [5] of the order of millimeters can be achieved through the designs for high bandwidth modulators on InP generic platform [6]. CS-SSB modulation is widely implemented in a dual-parallel Mach Zehnder modulator architecture[4] but has also been realized in a cascaded architecture enabling lower drive voltage and optical loss [7]. The performance of the FMCW transmitter depends on the optical power loss of the architecture and the extinction ratio of undesired sidebands and carrier relative to the sideband of interest. Fabrication limitations and wavelength-dependent imbalances result in differences in optical amplitudes between parallel arms of the architectures, degrading the performance. In the present work, we compare the tolerance of the parallel and cascaded architectures to imbalances in optical amplitudes through simulations.

Quadrature modulator architectures

Figure 1 and Figure 2 show the quadrature modulators with parallel architecture and cascaded architecture, respectively. The I and Q signals are 90 degrees out of phase. In

both figures, a pair of high-speed electro-optical phase modulators in a push-pull configuration are in series with DC electro-optical phase modulators (to tune the operating point and compensate optical path length mismatches). In each section, a single DC EOPM in either of the arms is sufficient to provide the desired phase shift. However, the resulting amplitude imbalance degrades the performance of the transmitter. Additional DC EOPMs are added to balance the optical losses in parallel paths. To realize carrier suppressed single sideband modulation, the parallel architecture utilizes more components than the cascaded architecture and has a slightly higher footprint. The additional DC phase modulators in the parallel architecture increase the control signals to be applied. Transfer functions of the individual components[7] are used to simulate the architectures in MATLAB. The components have ideal behaviour and do not include insertion loss , dispersion and voltage-dependent losses. As a result, the comparison between architectures is not limited to a particular platform. The input laser has a power of 0.5 mW. The system performance is quantified by extinction ratio (ER), which is the ratio of the power in the desired sideband to the power in the highest undesired tone. Another metric is the modulated to unmodulated power ratio (MUPR), defined as the ratio of the power in the desired sideband to the power of the unmodulated laser.

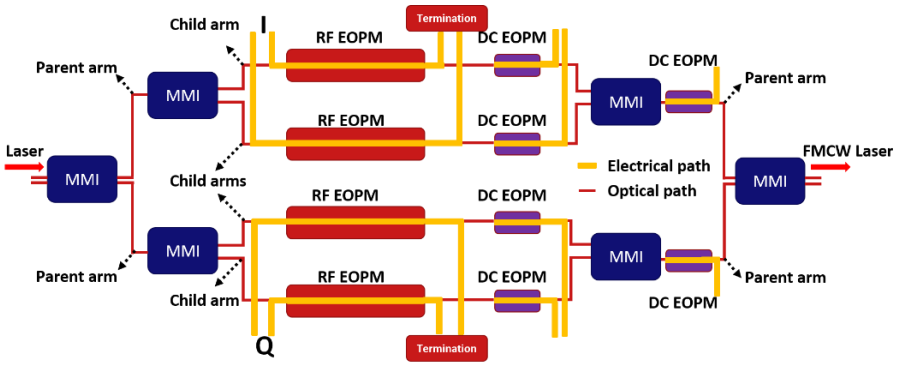

Figure 1. Quadrature modulator with parallel architecture. RF EOPM: RF electro-optic phase modulator. DC EOPM: DC electro-optic phase modulator. MMI: multi-mode interference coupler. I: in-phase signal, Q: quadrature phase signal.

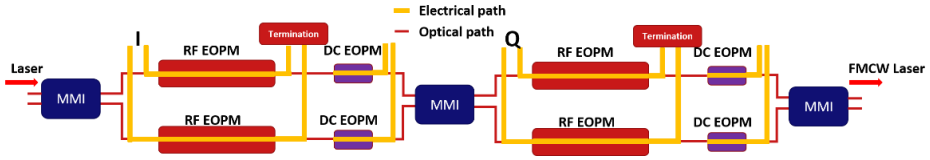

Figure 2. Quadrature modulator-Cascaded architecture. RF EOPM: RF electro-optic phase modulator. DC EOPM: DC electro-optic phase modulator. MMI: multi-mode interference coupler. I: in-phase signal, Q:quadrature-phase signal.

Figure 3(a) shows the extinction ratio (ER) and MUPR for cascaded and parallel architectures as a function of the RF drive voltage normalized to V_π. ER decreases with an increase in V_{RF} due to increased power present at other harmonics, while the MUPR initially increases due to an increase in the power present at the first sideband. For ER>20 dB, the cascaded architecture achieves the same extinction ratio as the parallel architecture at lower RF voltage drives along with higher MUPR. For example, at $V_{RF}= 0.2V_\pi$, the cascaded architecture has an ER of 29.2 dB and an MUPR of -4.92 dB. In contrast, at a higher voltage of $V_{RF}= 0.3V_\pi$, the parallel architecture has an ER of 28.13 dB with a lower MUPR of -7.52 dB. Figure 3(b) and Figure 3(c) show the output spectra of cascaded architecture and parallel architecture, respectively ($V_{RF}= 0.4V_\pi$, $f_{RF}= 1$ GHz). The third harmonic of the upper sideband is the dominant undesired term in both the

architectures. ER is a relative measure within the CS-SSB spectrum and does not vary with insertion loss of the components. However, the MUPR changes with the insertion loss of the individual components, and the MUPR curve has to be shifted down by the insertion losses of the components in one of the parallel paths from input to output. Semiconductor optical amplifiers available in the InP platform can be used to compensate for these losses.

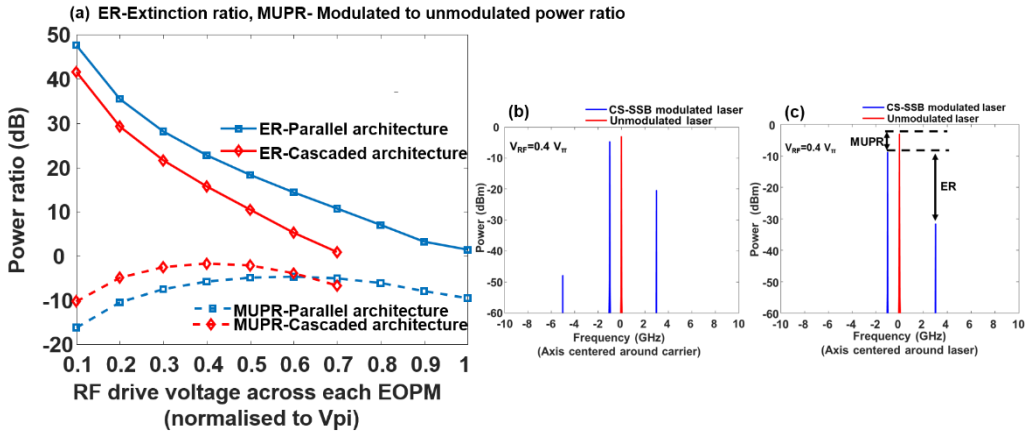

Figure 3 (a) ER (extinction ratio) and MUPR (modulated to unmodulated power ratio) as a function of RF drive voltage in parallel and cascaded MZM architectures. (b) Lower sideband of cascaded architecture at $V_{RF}=0.4\ V_{\pi}$, and (c) Lower sideband of parallel architecture at $V_{RF}=0.4\ V_{\pi}$

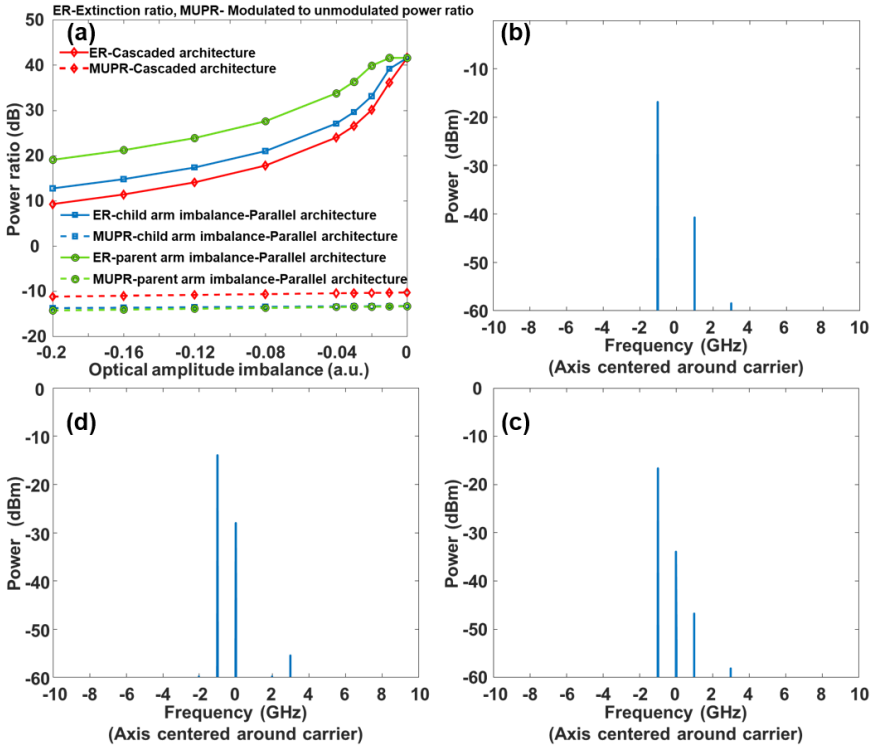

Figure 4 (a) ER (extinction ratio) and MUPR (modulated to unmodulated power ratio) dependence on optical amplitude imbalance ($V_{RF}=0.1\ V_{\pi}$) in cascaded architecture and parallel architecture ($V_{RF}=0.141\ V_{\pi}$). MUPR values for imbalances in child (green dashed line) and parent arms (blue dashed line) of parallel architecture almost overlap each other. Spectrum with an optical amplitude imbalance of -0.12 between (b) parent arms of parallel architecture, (c) child arms of parallel architecture, and (d) arms of cascaded architecture.

Effect of optical amplitude imbalance

Asymmetry in optical powers among parallel optical paths degrades ER of the system. In the parallel architecture, the arms can be identified as child arms (forming the I and Q MZMs) or parent arms (forming the outer MZM), as shown in Figure 1. Figure 4(a) shows the effect of introducing an optical amplitude imbalance(ΔE) in one of the parallel paths (as a factor of $(1+ \Delta E)$) on ER and MUPR. The RF drive voltages are adjusted to yield the same ER when no imbalance is present to compare the architectures. In the parallel architecture, the carrier is suppressed between the arms of the child MZM. Therefore, imbalances in the parent arms do not affect carrier suppression (Figure 4 (b). On the other hand, the imbalances in a child's arms lead to incomplete carrier suppression (Figure 4 (c)). Cascaded architecture has the highest sensitivity to imbalance (Figure 4 (d)). The amplitude imbalance where the ER falls to 20 dB is ~ -0.18 (~1.72 dB power imbalance) for the parent arms in a parallel architecture. For the child arms in the same architecture, the value is ~-0.09 (~0.82 dB power imbalance). In the cascaded architecture, the corresponding imbalance is ~-0.07 (~0.63 dB power imbalance).

Conclusions

The extinction ratio (ER) and modulated to unmodulated power ratio (MUPR) in cascaded and parallel architectures are analyzed through MATLAB simulations to evaluate their performance for FMCW LiDAR systems . For a given ER, the cascaded architecture requires lower RF drive power and has higher MUPR than the parallel architecture. However, the parallel architecture is more resilient to imbalance (~0.82 dB power imbalance for 20 dB ER) than the cascaded architecture (~0.63 dB power imbalance for 20 dB ER).

Acknowledgments

This work has received funding support from the European Union's Horizon 2020 program through the NewControl project under grant no. 826653.

References

[1] Y. Li and J. Ibanez-Guzman, "Lidar for Autonomous Driving: The Principles, Challenges, and Trends for Automotive Lidar and Perception Systems," *IEEE Signal Process. Mag.*, vol. 37, no. 4, pp. 50–61, Jul. 2020, doi: 10.1109/MSP.2020.2973615.

[2] M. Smit *et al.*, "An introduction to InP-based generic integration technology," *Semicond. Sci. Technol.*, vol. 29, no. 8, p. 083001, Jun. 2014, doi: 10.1088/0268-1242/29/8/083001.

[3] B. J. Isaac, B. Song, S. Pinna, L. A. Coldren, and J. Klamkin, "Indium Phosphide Photonic Integrated Circuit Transceiver for FMCW LiDAR," *IEEE J. Sel. Top. Quantum Electron.*, vol. 25, no. 6, pp. 1–7, Nov. 2019, doi: 10.1109/JSTQE.2019.2911420.

[4] P. Shi *et al.*, "Optical FMCW Signal Generation Using a Silicon Dual-Parallel Mach-Zehnder Modulator," *IEEE Photonics Technol. Lett.*, vol. 33, no. 6, pp. 301–304, Mar. 2021, doi: 10.1109/LPT.2021.3057986.

[5] E. Baumann *et al.*, "Comb-calibrated frequency-modulated continuous-wave ladar for absolute distance measurements," *Opt. Lett.*, vol. 38, no. 12, pp. 2026–2028, Jun. 2013, doi: 10.1364/OL.38.002026.

[6] A. Meighan, Y. Yao, M. J. Wale, and K. A. Williams, "Design of 100 GHz-class Mach-Zehnder modulators in a generic indium phosphide platform," in *2020 IEEE Photonics Conference, IPC 2020 - Proceedings*, Sep. 2020, pp. 1–2, doi: 10.1109/IPC47351.2020.9252410.

[7] M. Hasan, O. Jafari, X. Guan, L. A. Rusch, S. Larochelle, and T. Hall, "Integrated Optical SSB Modulation / Frequency Shifting Using Cascaded Silicon MZM," *IEEE Photonics Technol. Lett.*, vol. 32, no. 18, pp. 1147–1150, Sep. 2020, doi: 10.1109/LPT.2020.3014221.